A fate of nonlinear evolution of drift waves: Excitation of nonlinear breathers

Kosuga, Yusuke
Research Institute for Applied Mechanics, Kyushu University

Inagaki, Shigeru
Research Institute for Applied Mechanics, Kyushu University

Kawachi, Yuichi
National Institute for Fusion Science, National Institute of Natural Sciences

出版情報：Physics of Plasmas. 29 (12), pp.122301-1-122301-15, 2022-12-02. AIP Publishing
バージョン：

Physics of Plasmas

RESEARCH ARTICLE | DECEMBER 02 2022

A fate of nonlinear evolution of drift waves: Excitation of nonlinear breathers

Y. Kosuga ; S. Inagaki ; Y. Kawachi

Phys. Plasmas 29, 122301 (2022)
https://doi.org/10.1063/5.0122295

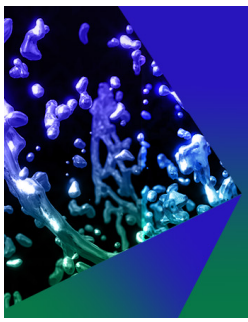

Physics of Plasmas ARTICLE scitation.org/journal/php

A fate of nonlinear evolution of drift waves: Excitation of nonlinear breathers

Cite as: Phys. Plasmas **29**, 122301 (2022); doi: 10.1063/5.0122295
Submitted: 23 August 2022 · Accepted: 7 November 2022 ·
Published Online: 2 December 2022

Y. Kosuga,[1,2,a)] S. Inagaki,[1,2,3] and Y. Kawachi[4,5]

AFFILIATIONS

[1]Research Institute for Applied Mechanics, Kyushu University, Kasuga, Fukuoka 816-8580, Japan
[2]Research Center for Plasma Turbulence, Kyushu University, Kasuga, Fukuoka 816-8580, Japan
[3]Institute of Advanced Energy, Kyoto University, Uji, Kyoto 611-0011 Japan
[4]National Institute for Fusion Science, National Institute of Natural Sciences, Toki, Gifu 509-5292 Japan
[5]Interdisciplinary Graduate School of Engineering Sciences, Kyushu University, Kasuga, Fukuoka 816-8580, Japan

[a)]Author to whom correspondence should be addressed: kosuga@riam.kyushu-u.ac.jp

ABSTRACT

We present the evidence that drift waves can develop into nonlinear breathers. The theoretical analysis predicts that drift waves with secondary flow can excite the nonlinear breather through modulational instability. It is found that the simultaneous modulation of both amplitude and phase is a relevant feature of breather excitation. These features are used to elucidate the excitation of drift breather in a linear plasma experiment. The drift breathers are found to be excited frequently and intermittently. The transient increase in the transport flux is also demonstrated. We argue that there exists a critical condition on the wave amplitude for breather excitation.

I. INTRODUCTION

A fascinating feature of turbulent plasmas is its tendency to self-organize a rich variety of structures or patterns from turbulence. These secondary patterns then determine the property of plasmas and play important roles in magnetic field dynamo,[1,2] plasma acceleration,[3] etc. Secondary patterns are also crucial for magnetic fusion, and it is now well established that drift wave turbulence nonlinearly generates zonal flows.[4–9] Zonal flows in turn regulate underlying fluctuations and play key roles in transition to the improved confinement.[10–12] While this is the case that secondary structures play beneficial roles for confinement, there is another class of secondary flows that deteriorate confinement.[13–17] For example, small-scale drift wave turbulence can drive radially elongated large-scale flows or streamers.[18–21] The excitation of radially elongated structures recently gains increasing attention due to their role in driving the edge collapse.[22,23] The list of secondary patterns explained here is not exhaustive and is indeed expanding. Recent studies report the formation of $E \times B$ staircases,[24,25] which may be viewed as a sequence of multiple transport barriers. These studies exemplify the nature of turbulent plasmas to excite various secondary structures and the impact of secondary patterns on confinement.

Another typical example of nonlinear pattern formation is perhaps given by nonlinear waves[26] in the system. Nonlinearity allows the accumulation of energy and steepens waves, while dispersion/dissipation provides stabilizing effects. The combination of the two processes leads to the excitation of a rich variety of nonlinear waves and associated dynamics. For example, when these two effects are balanced, stably propagating solitons can form, as reported for fluids and plasmas.[27–29]

An extreme case of nonlinear wave excitation may be illustrated by breathers, or in particular, rogue waves.[30,31] Here, a breather is characterized by a transient increase in wave amplitude. When the amplification exceeds the factor of 2, the breather is called a rogue wave. The excitation of rogue wave is originally reported from ocean, and its existence is confirmed in water tank experiment.[32] The excitation of rogue waves is not limited to ocean waves: Rogue waves are very universal and excited for various systems (see Table I), such as capillary waves[33] and optical fibers.[34] Breathers are also reported for plasmas including negative ions,[35] dusts,[36] and/or quantum plasmas.[37,38] Alfvén/Whistler waves are also predicted to develop into breathers.[39] Common ingredients for these different problems are the nonlinear evolution of the envelope of dispersive underlying waves. When the nonlinearity is strong enough, the envelope becomes modulationally unstable, and the nonlinear breathers are excited. The excitation of breathers is a consequence of the nonlinear evolution of dispersive waves.

TABLE I. The nonlinear evolution of various dispersive waves. The nonlinear interaction leads to the modulation of the wave envelope, and the dynamics is commonly described by nonlinear Schrödinger equation.

Dispersive	Surface wave	Light	Langmuir wave	Drift wave
waves	$\omega^2 = gk$	$\omega = \frac{ck}{n_{ref}}$	$\omega^2 = \omega_{pe}^2(1 + 3k^2\lambda_D^2)$	$\omega = \frac{\omega_{*e}}{1+\rho_s^2 k_\perp^2}$
Nonlinearity	Surface elevation	Medium response $n_{ref} \propto \sqrt{\epsilon(E)}$	Ponderomotive force Ion acoustic coupling	Reynolds stress Large-scale flows pumped
Feedback	Modulation of sea surface	NL refraction Self-focusing	Refraction by modulated Density field	Shearing by flows

Drift wave in magnetized plasmas is no exception for such a dispersive wave. Indeed, nonlinear waves are excited,[28,29] and more recent works report the observation of solitary perturbation associated with the sudden release of free energy in fusion plasmas.[22,23,40] As discussed above, breathers/rogue waves may be excited due to the nonlinear evolution of dispersive drift waves. The excitation of rogue waves in fusion plasmas poses several challenges from confinement perspective. For example, since the transport flux is proportional to the square of the amplitude, rogue waves may increase the flux by a factor of 4 or so. More seriously, this enhancement happens transiently. This transient increase in the transport flux is undesirable from the engineering point of view and may be a matter of concern for the heat load on divertor.[41] Hence, it is an important issue to clarify whether rogue waves are excited in magnetized plasmas, and if so, to develop a way to predict its excitation and/or to regulate rogue waves in magnetized plasmas.

The purpose of this work is to provide an evidence that drift waves can nonlinearly develop into breathers (or rogue waves), which we refer to as drift breathers. In doing so, a challenge is to distinguish the contribution of breathers from other intermittent bursts in the data. Previous works on breather excitation used theoretical waveform to characterize the sudden increase in the amplitude. However, since magnetically confined plasmas also exhibit wide variety of intermittent bursts, such as avalanches,[42–44] blobs,[45–47] tongue events,[40] solitary perturbation, and the pedestal collapse,[22] amplitude alone may not be sufficient to extract rogue wave excitation. A more stringent criterion is necessary.

To address this issue, we first discuss relevant features of breathers predicted from theory. As demonstrated for the ocean rogue waves, nonlinear breathers are excited through modulational instability of the underlying wave and its nonlinear evolution. A similar story can be developed for the excitation of drift breathers, and their excitation is formulated by nonlinear Schrödinger (NLS) equation. While the original NLS has been derived for the description of Bose–Einstein condensation, the model is applicable for the description of the nonlinear evolution of dispersive waves (Table I). In fusion plasmas, NLS has been applied to describe the excitation of flows.[18,48–51] In this work, we focus on the nonlinear stage of the modulational growth, which is often analyzed by using exact solutions for NLS. Although several solutions are cited from literatures (see Table II) and used to characterize the spatiotemporal dynamics of the nonlinear evolution, assumptions behind their derivation are unclear, and thus, the physics associated with each exact solution is obscured. By revisiting the derivation of the exact solutions, we show that breather solutions are obtained under a constraint on the real and imaginary part of the complex envelope of waves. Physically, this leads to a unique behavior in the phase modulation of the envelope. We argue that this phase evolution is an origin of the transient behavior of nonlinear breathers.

While the model is a straightforward extension of the NLS story for ocean rogue waves, a non-trivial part is to use this waveform to detect drift breathers in experimental data. As reported from previous studies on water tank experiments, surface rogue waves are experimentally observed by analyzing amplitude evolution. In this work, we provide a thorough evidence for breather excitation by using both temporal and spatial data. This is made possible by a unique multipoint measurement in a basic magnetized plasma experiment, PANTA.[55,56] Various intermittent fluctuations are excited in magnetized plasmas. We show that breather excitation can be extracted by analyzing both amplitude and phase modulation. As a consequence of the breather excitation, fluctuation amplitude transiently increases. This leads to the transient amplification of transport flux. This is also confirmed in data analysis. While we provide a case that drift breathers are excited in magnetized plasmas, drift breathers are not always excited. The condition for its excitation is also discussed.

The remaining of the paper is organized as follows. Section II presents the theory of drift breather excitation. The excitation is formulated using the modulational analysis. The nonlinear spatiotemporal waveform is obtained. The predicted waveform is used to seek for footprints of drift breather excitation in Sec. III. Section IV is for the conclusion and discussion.

II. THEORY FOR BREATHERS IN DRIFT WAVE SYSTEM

A. Model

Breathers are excited as a consequence of the nonlinear evolution of underlying waves. To demonstrate this in magnetized plasmas, we consider drift wave as a specific example. In a typical magnetized plasma with the magnetic field in the z direction and with the density gradient in the radial direction, the dynamics of drift waves may be modeled by Hasegawa–Mima equation

$$\mathcal{L}\phi = \mathcal{N}, \tag{1}$$

$$\mathcal{L} = \partial_t(1 - \rho_s^2\nabla_\perp^2) + v_{*e}\partial_y, \tag{2}$$

$$\mathcal{N} = -c_s\rho_s\hat{z} \times \nabla\bar{\Psi} \cdot \nabla(1 - \rho_s^2\nabla_\perp^2)\phi - c_s\rho_s(\hat{z} \times \nabla\phi) \cdot \nabla\bar{N}. \tag{3}$$

Here, ϕ is the normalized potential for drift wave fluctuation (i.e., $e\phi/T_e \to \phi$), $\bar{\Psi}$ is the normalized potential for large-scale flows, and $\bar{N}$ is the normalized density field associated with the large-scale flows. ρ_s is the ion sound Larmor radius, c_s is the ion sound speed, and v_{*e} is the drift velocity. $\perp$ denotes the direction perpendicular to the

TABLE II. Nonlinear waves obtained in nonlinear Schrödinger equation. Key features and assumptions behind each solution are summarized. This work discusses the relevance of the phase modulation in the breather excitation and provides an evidence of Akhmediev breather excitation in drift wave system.

Nonlinear solutions	Akhmediev breather Eq. (28)	Peregrine breather Eq. (36)	Kuznetsov–Ma breather Eq. (42)	Envelope soliton Eq. (44)
Feature	Localized in time Periodic in space See Fig. 2	Localized both in time and space See Fig. 7	Localized in space Periodic in time See Fig. 9	Stable propagation Slight modulation See Fig. 10
Key assumptions	Eq. (22) Constraint on phase → Phase modulation	A special case of Akhmediev breather $\nu \to 0$	Eq. (37) or $\nu \to i\mu$	Propagating solution $A(y-c_1t)$, $\vartheta(y-c_2t)$
Observation	Water tank,[32] optics,[52] unmagnetized plasma[35] (ion acoustic wave with negative ions) Magnetized plasma (drift wave): this work		Water tank,[53] optics[54] Plasma: TBD	See, e.g., Ref. 26 and references therein

magnetic field. To simplify the analysis below, we use a local coordinate (x, y), which corresponds to (r, θ), respectively. In this system, the electron diamagnetic direction corresponds to the positive y direction. The left-hand side is the linear evolution of drift waves, while the right-hand side represents the nonlinear evolution of drift waves due to the coupling to the large-scale flows. Note that the linear analysis is straightforward and the dispersion relation is obtained from $\mathcal{L}(\omega, \mathbf{k}) = 0$, which gives

$$\omega = \frac{\omega_{*e}}{1+\rho_s^2 k_\perp^2}. \tag{4}$$

Here, $\omega_{*e} = k_y v_{*e}$. The dispersion relation prescribes the typical wave properties of drift waves, including the propagation in the electron diamagnetic direction, the group velocity, and the wave dispersion.

The nonlinear evolution of drift wave can be formulated by considering the envelope modulation. The detailed derivation is available in the literature,[18,48,49,57] and here, we briefly outline the relevant steps. We first write the wave field as

$$\phi = \mathrm{Re}(\psi e^{i\mathbf{k}\cdot\mathbf{x}-i\omega t}), \tag{5}$$

where ϕ is the normalized electrostatic potential, that is, $e\phi/T_e \to \phi$, and ψ is the complex envelope. The underlying drift waves nonlinearly interact and introduce slow modulation. Here, the slow means

$$\left|\frac{\partial_t \psi}{\psi}\right| \ll \omega, \quad \left|\frac{\nabla\psi}{\psi}\right| \ll |\mathbf{k}|, \tag{6}$$

which defines a small parameter for the expansion, that is,

$$\epsilon \sim \frac{|\nabla\psi|}{|\mathbf{k}\psi|} \sim \frac{|\partial_t\psi|}{|\omega\psi|}. \tag{7}$$

Using this parameter, we perform the reductive perturbation expansion to obtain the hierarchy of the wave evolution. In this approach, we expand the time and space as $\mathbf{x} \to \mathbf{x} + \epsilon\mathbf{X} + \cdots$ and $t = t + \epsilon T + \epsilon^2\tau + \cdots$. The time variable is expanded up to the second order to obtain a non-trivial evolution, as shown later. These lead to

$$\frac{\partial}{\partial\mathbf{x}} \to \frac{\partial}{\partial\mathbf{x}} + \epsilon\frac{\partial}{\partial\mathbf{X}}, \quad \frac{\partial}{\partial t} \to \frac{\partial}{\partial t} + \epsilon\frac{\partial}{\partial T} + \epsilon^2\frac{\partial}{\partial\tau}. \tag{8}$$

Thus, the slow evolution is described by $\mathbf{X}$, T, and τ. The operator $\mathcal{L}$ can be expanded in terms of ϵ. The lowest order gives a dispersion relation via $\mathcal{L}_0(\omega, \mathbf{k}) = 0$. The first-order equation is

$$\left(\frac{\partial\mathcal{L}_0}{\partial\omega}\frac{\partial}{\partial T} + \frac{\partial\mathcal{L}_0}{\partial\mathbf{k}}\cdot\frac{\partial}{\partial\mathbf{X}}\right)\psi = 0. \tag{9}$$

Since $\mathbf{v}_{gr} = (\partial\mathcal{L}_0/\partial\mathbf{k})/(\partial\mathcal{L}_0/\partial\omega)$, the first-order dynamics corresponds to the propagation at the group velocity. This can be eliminated by going to the moving frame. The nontrivial dynamics is obtained at the second order, as

$$\left(i\frac{\partial\mathcal{L}_0}{\partial\omega}\partial_\tau + \frac{1}{2}\frac{\partial^2\omega}{\partial k_i\partial k_j}\partial_i\partial_j\right)\psi = \mathcal{N}(\psi, \bar{\Psi}, \bar{N}). \tag{10}$$

Here, the repeated indices are summed over $i, j = X, Y$. This equation is closed by adding the evolution of the large-scale fields

$$(\epsilon\partial_\tau - \mathbf{v}_g\cdot\nabla)\nabla_\perp^2\bar{\Psi} = 2\rho_s^2\omega_{ci}\left[k_x k_y(\partial_X^2 - \partial_Y^2) + (k_y^2 - k_x^2)\partial_{XY}\right]|\psi|^2, \tag{11}$$

$$(\epsilon\partial_\tau - \mathbf{v}_g\cdot\nabla)\bar{N} + v_{*e}\partial_Y\bar{\Psi} = 0. \tag{12}$$

These coupled equations describe the nonlinear evolution of dispersive drift wave envelope due to the modulation induced by large-scale fields. The set of equation can be further simplified by focusing on the anisotropic modulation. If we consider a streamer as an example, this corresponds to the larger modulation in the poloidal direction, $\partial_Y \gg \partial_X$. In such a case, the set of equation reduces to the 1D nonlinear Schrödinger equation (NLS)

$$i\partial_\tau\psi + \alpha\partial_Y^2\psi + \beta|\psi|^2\psi = 0. \tag{13}$$

Here, the term with the spatial derivative is related to the wave dispersion, and the coefficient is given by

$$\alpha = \frac{1}{2}\frac{\partial^2\omega}{\partial k_y^2}. \tag{14}$$

The nonlinear term is due to the coupling to the flows

$$\beta = c_s k_x \frac{2\rho_s^2 k_x k_y c_s}{v_{gy}} \left(1 - \frac{v_{py}}{v_{gy}}\right). \tag{15}$$

The dependence on $k_x k_y$ is reminiscent of flow coupling through the Reynolds stress, $\langle \tilde{v}_x \tilde{v}_y \rangle$. Hereafter, the slow variable is written as $\tau \to t$ and $Y \to y$ to simplify the notation.

NLS appears in the wide variety of the physical problems (Table I). In each system, the nonlinear evolution of underlying dispersive waves is formulated. Due to the nonlinear interaction, the underlying waves introduce nonlinear evolution, which feedback onto the original wave via modulation. The entire nonlinear evolution is modeled as the nonlinear evolution of envelope of the wave, which is described by the nonlinear Schrödinger equation. In plasmas, this framework was first developed for Langmuir waves, with coupling to ion acoustic waves via the ponderomotive force.[31] Ion acoustic waves in turn modulated density field and Langmuir waves are refracted in this case. This leads to the nonlinear evolution of Langmuir envelope. A similar story can be developed in fusion plasmas.[18,48,49] In this case, drift waves nonlinearly exert Reynolds stress to drive larger-scale shear flows. The flows then modulate underlying drift waves by shearing, and the resulting nonlinear evolution of drift wave envelope is formulated in terms of NLS.

NLS can be used to formulate the pumping of large-scale flows by drift waves through modulational instability. We first note that a uniform solution can be found in NLS, $\psi = A_0 \exp(i\beta A_0^2 t)$. This corresponds to the nonlinear phase shift of the underlying waves. Perturbing this homogeneous solution, we can obtain the dispersion relation for the modulation as

$$\Omega^2 = \alpha^2 q^4 - 2\alpha\beta A_0^2 q^2. \tag{16}$$

Here, Ω and q are the frequency and the wave number of the modulation, respectively. The modulation becomes unstable when $\alpha\beta > 0$. The growth rate is maximum at $q^2 = \beta A_0^2/\alpha$, with the growth rate given by $\gamma_{mod}^2 = \beta^2 A_0^4$. The perturbed amplitude grows, and inhomogeneous wave field develops. As a consequence, the modulated drift waves exert Reynolds stress to drive large-scale flows. Alternatively, modulational instability can be viewed as an energy spread of the pump wave in the wave number space.[58] The energy stored in the pump wave is modulated and can be transferred to sidebands. Since modulational instability induces the energy spread in the spectral space, this leads to the condensation of the energy in the real space. The pumping of large-scale flows via underlying waves is also confirmed in experiments by bi-spectrum analysis.[6,8,14]

Here, let us note that the modulational instability in plasmas is also discussed in the context of the quasi-Chaplygin media, which covers wide range of so-called negative compressible type phenomena.[59] In the cited work, the modulation of Langmuir wave is also modeled by NLS. The nonlinear stage of the modulational instability is also studied, which covers the formation of stably propagating solitons and the collapse in the three-dimensional case. In a related vein, we note that the nonlinear stage of the modulational instability may be modeled via shock wave-like structures.[60] Unlike these works, here we describe a transient feature of the nonlinear evolution of the modulational instability of drift waves via the excitation of a nonlinear breather. This point is elaborated in Sec. II B.

B. Drift breather solution

The envelope of the drift waves can accumulate in space via modulational instability. The fate of this process can be described by the nonlinear analysis of NLS. In order to characterize the entire nonlinear evolution of the wave envelope, here we discuss the nonlinear, nonperturbative analysis of NLS. In this section, we obtain a so-called breather solution of NLS. As explained in detail later, a breather is a nonlinear wave that exhibits transient increase in the wave amplitude. Unlike the linear wave whose energy is uniformly distributed over the space and time, the nonlinear breather is characterized by the local accumulation of the energy. This is often caused by modulational instability. Interestingly, this accumulated energy is radiated again, and the entire process appears as a transient increase in the wave energy. Through this entire process, the wave looks as if they breathe; hence, the name follows. Mathematically, the breather solution is obtained without assuming propagating solutions in the form of $A(x - vt)$, etc. Thus, breather solutions are different from stably propagating solitons.

Before starting a detailed analysis, let us summarize some features that the solution of NLS should satisfy, even in the nonlinear regime. First, we note that by setting $t \to -t$, NLS reads

$$-i\partial_t \psi(-t) + \alpha\partial_y^2 \psi(-t) + \beta|\psi(-t)|^2 \psi(-t) = 0. \tag{17}$$

On the other hand, taking the complex conjugate of NLS gives

$$-i\partial_t \psi^*(t) + \alpha\partial_y^2 \psi^*(t) + \beta|\psi^*(t)|^2 \psi^*(t) = 0. \tag{18}$$

For these two equations to be satisfied for arbitrary t, we need to have $\psi(-t) = \psi^*(t)$. For example, the homogeneous solution discussed above, $\psi = A_0 \exp(i\beta A_0^2 t)$, satisfies this property. This gives an interesting property of the nonlinear evolution described by NLS. To show this, we note another important property of NLS, namely, the conservation of wave energy. This can be easily derived, and the result is

$$\partial_t |\psi|^2 + \partial_y J = 0. \tag{19}$$

Here, the flux J is given by

$$J = i\alpha(\psi\partial_y\psi^* - \psi^*\partial_y\psi) = 2\alpha \mathrm{Re}(i\psi\partial_y\psi^*). \tag{20}$$

Using $\psi(-t) = \psi^*(t)$, we have $J(-t) = -J(t)$. Thus, the flux is odd in time and flips its sign at the late stage of evolution. As depicted in Fig. 1, this implies that even when the wave energy initially grows, this accumulated energy will be radiated away eventually. The entire process may be viewed as a transient excitation of the localized wave energy. Thus, very generally, we expect that the nonlinear behavior described by NLS leads to a breathing nonlinear oscillation in time. We note that there is an exception for this. This property may not hold for the case of wave collapse.[61] In this case, once modulational instability is triggered, the wave energy grows and leads to a finite time singularity. At this point, a different physics comes into play to cause a dissipation at small scales, etc. The dynamics may not be long enough for the flux to flip sign. For the case of 1D NLS, the collapse does not occur, and instead, breathing oscillation will be excited, as shown below. We finally note that $J(0) = 0$ since $J(t)$ is odd in time. This implies that the wave energy reaches a maximum value at $t = 0$.

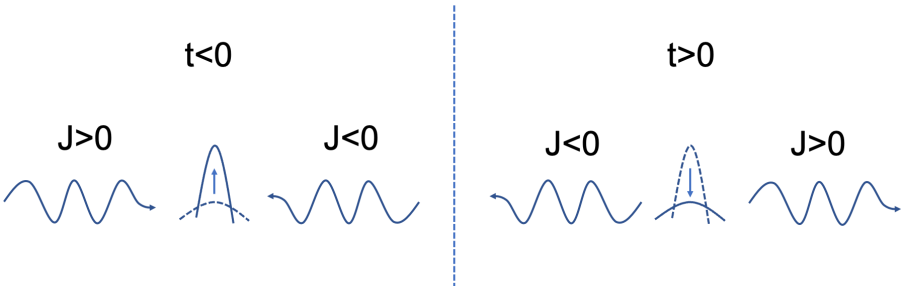

FIG. 1. Typical behavior of flux at $t<0$ and $t>0$. Even when the flux converges and the energy accumulates in space at $t<0$, the direction of the flux is inverted and the accumulated energy is redistributed.

A nonlinear solution to NLS can be found exactly. To show this, we write $\psi = A_0 \exp(i\beta A_0^2 t)(u+iv)$ where $u(t,y)$ and $v(t,y)$ are real. Then, NLS reduces to

$$\partial_t u + \alpha\partial_y^2 v - \beta A_0^2 v + \beta A_0^2(u^2+v^2)v = 0, \tag{21a}$$

$$\partial_t v - \alpha\partial_y^2 u + \beta A_0^2 u - \beta A_0^2(u^2+v^2)u = 0. \tag{21b}$$

Note that $u(-t) = u(t)$ and $v(-t) = -v(t)$, which are required from $\psi(-t) = \psi^*(t)$. Note also that linearizing these equations via $u = 1+\delta u$ and $v = \delta v$ yields the dispersion relation discussed above. Several exact solutions are known to exist for Eqs. (21a) and (21b). Among others, here we focus on the solution periodic in space, which is compatible with the boundary condition for drift waves, nonlinear envelopes, and experiments. The solution can be obtained by assuming

$$\frac{v}{u+1} = \frac{\sqrt{2-\nu^2}}{\nu}\tanh(\beta A_0^2\sigma t), \tag{22}$$

where $\sigma = \nu\sqrt{2-\nu^2}$. This relation sets a constraint on the evolution of the real part and the imaginary part of the wave envelope. In this sense, the solution obtained in this manner has a characteristic feature in the phase evolution. This point will be elaborated later. ν is a parameter to characterize the form of the nonlinear solution. The existence of the solution requires $\nu^2 < 2$. Substituting this relation, we have

$$\partial_t u + \beta A_0^2 \frac{\sigma}{\nu^2}\tanh(\beta A_0^2\sigma t)(u+1)(u+1-\nu^2) = 0. \tag{23}$$

This can be integrated to give

$$u = -1 + \frac{\nu^2\cosh(\beta A_0^2\sigma t)}{\cosh(\beta A_0^2\sigma t) - C(y)}, \tag{24}$$

$$v = \frac{\sigma\sinh(\beta A_0^2\sigma t)}{\cosh(\beta A_0^2\sigma t) - C(y)}, \tag{25}$$

where $C(y)$ is a integration constant independent of time. $C(y)$ is determined by substituting these expressions into the original equations. After straightforward algebra, we obtain

$$\frac{2\alpha}{\sigma^2\beta A_0^2}(\partial_y C)^2 + \frac{2\nu^2}{\sigma^2}C^2 = 1. \tag{26}$$

Thus, we have

$$C = \sqrt{\frac{\sigma^2}{2\nu^2}}\cos(Ky), \tag{27}$$

where $K = \nu\sqrt{\beta A_0^2/\alpha}$ is the amplitude-dependent wave number of the envelope. The periodic boundary condition requires $K2\pi r = 2\pi p$, where p is an integer. This constraint gives the parameter ν in terms of physical variables, such as the wave amplitude, dispersiveness, and nonlinear coefficient. Then, the nonlinear spatiotemporal pattern of the envelope, also known as the Akhmediev breather, is given by

$$\psi(t,y) = A_0 e^{i\beta A_0^2 t} \times \left(\frac{\sqrt{2}\nu^2\cosh(\beta A_0^2\sigma t) + i\sqrt{2}\sigma\sinh(\beta A_0^2\sigma t)}{\sqrt{2}\cosh(\beta A_0^2\sigma t) - \sqrt{2-\nu^2}\cos(Ky)} - 1\right). \tag{28}$$

The solution exists only for $\nu^2 < 2$. Thus, the nonlinear wave can be excited only when

$$2\alpha\beta A_0^2 > \frac{\alpha^2 p^2}{r^2}. \tag{29}$$

Note that the above condition is consistent with the excitation condition for the modulational instability. Thus, when the modulational instability is triggered, the nonlinear solution exists. It is then likely that modulationally unstable wave would evolve into the nonlinear wave described by Eq. (28).

The excitation of the nonlinear wave leads to the amplification of the background wave amplitude. As discussed above, this maximum value will be at $t=0$. In this case, the wave amplitude is amplified as

$$\frac{\psi(t=0,y)}{A_0} = \frac{\sqrt{2}\nu^2}{\sqrt{2}-\sqrt{2-\nu^2}\cos(Ky)} - 1. \tag{30}$$

This also gives the location for the maximum amplitude, which is at $\cos(Ky) = 1$. Depending on the system size and plasma parameters, modulations grow at multiple locations in space. At these locations, the amplification factor is given as

$$F_A = \frac{\sqrt{2}\nu^2 - \sqrt{2} + \sqrt{2-\nu^2}}{\sqrt{2}-\sqrt{2-\nu^2}}. \tag{31}$$

For $0 < \nu^2 < 2$, F_A ranges from 1 to 3. For the special case of $F_A > 2$, the nonlinear wave is called a rogue or freak wave. In principle, rogue waves can increase the transport flux by the factor ranging from 4 to 9. Even for the amplification below that of rogue waves, transport flux may be doubled in fusion plasmas. In this sense, while the excitation of rogue waves is a serious concern for fusion plasmas, even mild breather will have a visible impact on the transport flux. In this work, we use a general name of breather, or a drift breather to indicate the transient increase in wave energy described by Eq. (28), including the case of rogue waves.

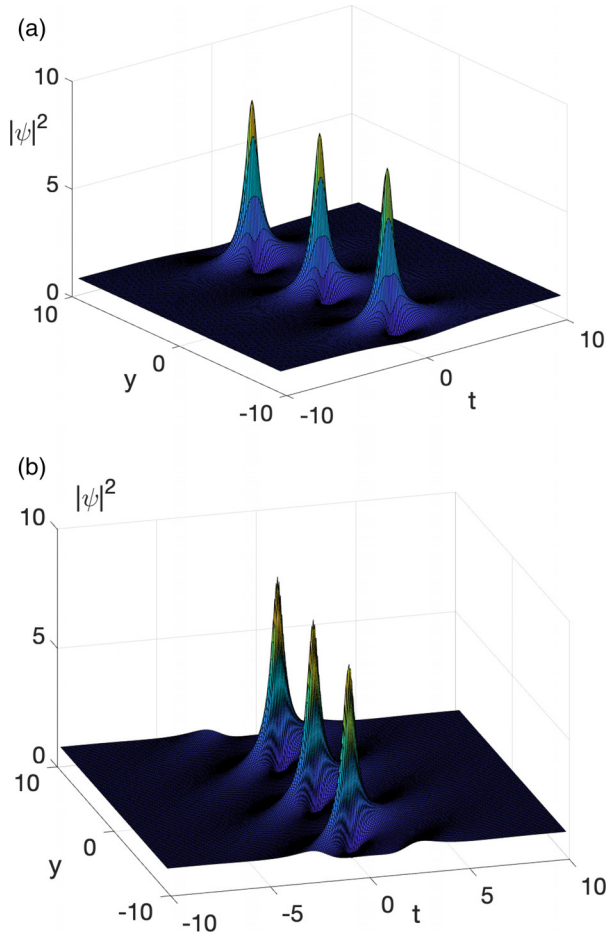

FIG. 2. The spatial–temporal landscape of the wave energy in the wave frame (a) and in the laboratory frame (b). The amplification of the wave energy is localized in space. In the laboratory frame, the condensation appears at each spatial location and each event propagates at the group velocity.

The spatiotemporal behavior described by Eq. (28) is illustrated here. Normalized coordinates are used as $Ky \to y$, $\beta A_0^2 t \to t$, $\psi/A_0 \to \psi$. $\nu = 0.5$ is used as a typical example. This gives the amplification factor $F_A = 2.87$, or in terms of the wave energy $F_A^2 = 8.24$. The spatiotemporal landscape of the wave energy surface is given in Fig. 2. The wave energy accumulates at three locations. At each location, the wave energy grows and then disappears. Since NLS is formulated in the wave frame, the pattern in the laboratory frame is also shown in Fig. 2(b). In the laboratory frame, the excitation is along the trajectory of the wave propagating at the group velocity. This pattern in the laboratory frame is later used to compare against other nonlinear waves excited in the system.

We can have a closer look at the wave evolution by slicing the landscape [Fig. 2(a)]. We start by describing the temporal evolution at fixed spatial points, as shown in Fig. 3. The wave envelope is initially uniform, and the modulation starts growing. Then, the wave energy enters the nonlinear stage of the evolution. At this stage, the wave energy saturates at a maximum value

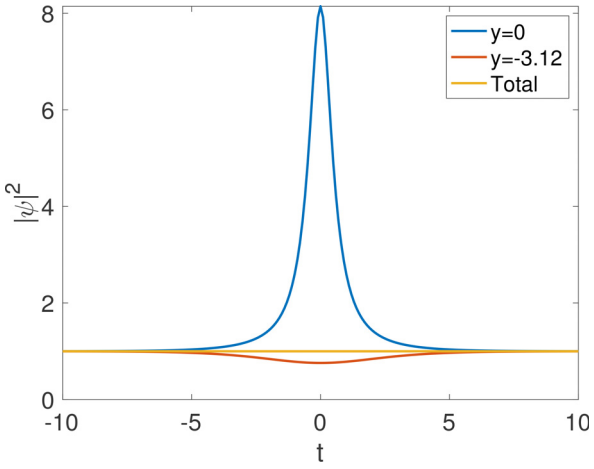

FIG. 3. The time evolution of the energy at fixed spatial points. The amplification of the wave energy (at $y = 0$) is made possible by accumulating energy from other spatial locations ($y = -3.12$) via modulational instability. The spatial averaged energy is conserved during the entire evolution.

and then decays. Thus, the excitation of the nonlinear wave is localized in time and appears as a transient event. In this excitation process, the energy needs to be conserved. The wave envelope at $y = 0$ grows by condensing energy from other locations. For example, the energy at $y = -3.12$ is depleted, as shown in red. This is a typical symptom of the modulational growth. The total energy integrated over the space, $\int dy|\psi|^2$, is conserved during the entire evolution, as indicated by the yellow curve.

The dynamics of the spatial pattern is shown in Figs. 4(a) and 4(b). Here, the case with three growing locations is shown. At the initial stage, the wave envelope is slightly modulated [the blue curve in Fig. 4(a)] and grows (the red and yellow curves) through modulational instability. Here, the growth happens at the three different spatial locations. The condensation of the wave energy discussed above is clearly shown. At the later stage, the growth saturates and decays subsequently [Fig. 4(b)]. Interestingly, we note that when the amplitude reaches the maximum, the wave energy is depleted to zero at some locations. It appears that no more energy is available for the growth at this point and the modulational growth stops. Once the wave energy attains the maximum value, the energy condensed at each location is redistributed.

Having discussed the spatiotemporal behavior of the breather energy, we now turn to the analysis of the energy flux associated with the excitation of breather oscillation. In the case discussed here, the flux can be calculated as

$$J = 2\sqrt{2}A_0^2\alpha\sigma\sqrt{2-\nu^2}K \times \frac{\sin(Ky)\sinh(\sigma\beta A_0^2 t)}{\left(\sqrt{2}\cosh(\beta A_0^2\sigma t) - \sqrt{2-\nu^2}\cos(Ky)\right)^2}. \quad (32)$$

The flux is explicitly odd in time. The typical behavior is plotted in Fig. 5. For $t < 0$, the flux converges into several points ($y = 0, \pm 6.28$). The wave energy accumulates in these points and grows. This is consistent with the spatial evolution discussed in Fig. 4(a). The flux becomes zero at $t = 0$, and the wave energy reaches maximum. At the later stage

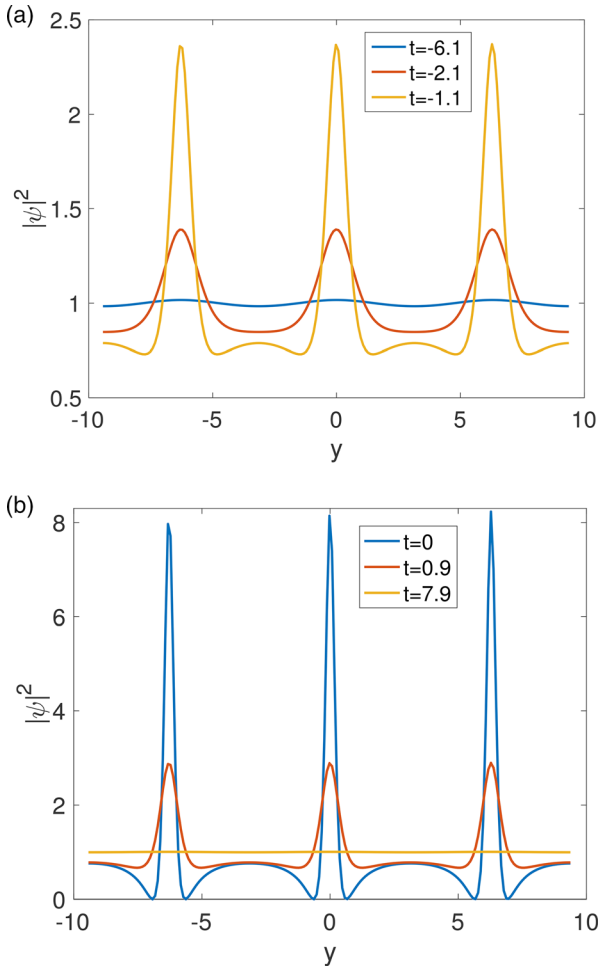

FIG. 4. The spatial pattern of the nonlinear breather. The wave energy is condensed via Modulational instability at three locations in this example. Once the energy reaches the maximum value at $t=0$, the energy is redistributed over the space.

($t>0$), the flux has diverging pattern. Spatially condensed wave energy is then distributed over the space, which is consistent with Fig. 4(b).

The excitation of drift breather leads to the transient increase in the amplitude, as discussed above. This amplification reaches up to 3 and may be visible in the time series. While this is one aspect of drift breathers, another important feature is that the drift breather excitation involves the modulation of phase as well. Writing $\psi = A\exp(i\vartheta)$, NLS reduces to the coupled nonlinear PDE for amplitude and phase as

$$\partial_t A + 2\alpha\partial_y\vartheta\partial_y A + \alpha A\partial_y^2\vartheta = 0, \tag{33a}$$

$$A\partial_t\vartheta - \beta A^3 - \alpha\partial_y^2 A + \alpha A(\partial_y\vartheta)^2 = 0. \tag{33b}$$

The amplitude and phase are related to the function u and v introduced above via

$$A = A_0\sqrt{u^2+v^2}, \tag{34a}$$

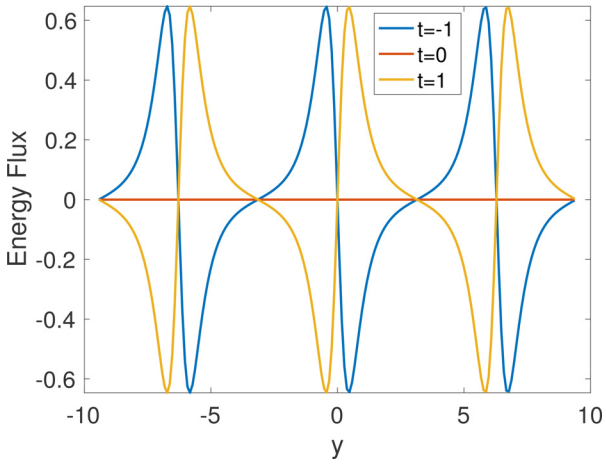

FIG. 5. The spatial pattern of the energy flux associated with the breather excitation. At $t<0$, the flux has a converging pattern, and hence, the wave energy grows. When the wave energy reaches the maximum at $t=0$, the flux is zero and inverted at $t>0$. At $t>0$, the energy flux has a diverging pattern and the condensed energy decays.

$$\tan(\vartheta - \beta A_0^2 t) = \frac{v}{u}. \tag{34b}$$

The phase of the envelope indeed provides several kinds of useful information. For example, the inhomogeneous phase field drives the wave energy flux as

$$J = 2\alpha A^2\partial_y\vartheta. \tag{35}$$

Since $\partial_y A$ is small at the location with the maximum amplitude, the phase curvature determines whether the location acts as a source or sink of the wave energy, that is, $\partial_y J \propto \partial_y^2\vartheta$. Note also that the flip of the energy flux is due to the phase evolution. This leaves a direct footprint in the time series. As an illustration, we consider the modulated drift wave with the frequency of the carrier 5 times faster than the envelope. The entire time evolution, including the phase of the carrier and the envelope, is shown in Fig. 6. The amplitude modulation is quite visible. At the same time, the phase of the oscillation is also modulated. For the reference, the underlying harmonic oscillation is depicted in red. The time series oscillates in phase initially. After the excitation of the drift breather, the phase of the time series is shifted. The simultaneous modulation of the envelope amplitude and phase is a useful footprint of drift breather excitation. This feature may be used to distinguish the excitation of drift breathers from other intermittent bursts in fusion plasmas. We provide the evidence of the simultaneous modulation in experiments later.

C. Other candidates for breather excitation

We have described the excitation of nonlinear breathers by using an exact solution for NLS, Eq. (28). Other exact solutions can be obtained, and here, for completeness we discuss some examples that are used for the study of breather excitation in water tank experiment, etc.

We first introduce the Peregrine breather solution.[32] This is indeed a special class of Akhmediev breather solution discussed above. By taking $\nu \to 0$, Eq. (28) reduces to

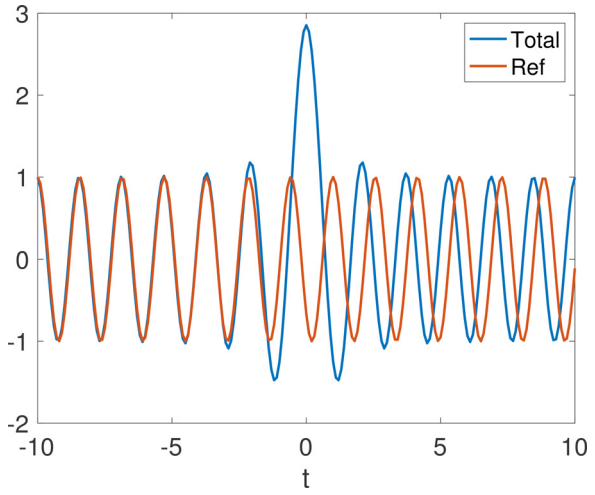

FIG. 6. The temporal evolution of the time series, including the carrier and the envelope. Here, the carrier frequency is taken as the 5 times of that of the envelope. The breather excitation is clear in the amplitude. The modulation of the phase is also visible, as shown as the shift between the total and the reference.

$$\psi(y,t) \to A_0 e^{i\beta A_0^2 t}\left(\frac{4(1+2i\beta A_0^2 t)}{1+2\beta^2 A_0^4 t^2 + 2A_0^2(\beta/\alpha)y^2} - 1\right). \tag{36}$$

The energy landscape is given in Fig. 7. Here, the same normalization is used. The Peregrine breather is localized both in time and space. The amplification factor is given by 3. The excitation of Peregrine breather is reported for surface waves of fluids and observed in water tank experiments.[32]

Another unique nonlinear breather is derived by Kuznetsov and Ma.[30] This solution can be obtained by assuming

$$\frac{v_{KM}}{u_{KM}+1} = \frac{\rho}{\mu^2}\tan(\beta A_0^2 \rho t), \tag{37}$$

where $\rho = \mu\sqrt{2+\mu^2}$. This also corresponds to the case with $\nu = i\mu$, where ν is the parameter introduced for Akhmediev breathers. In this case, Eqs. (21a) and (21b) reduce to

$$\partial_t u_{KM} + \beta A_0^2 \frac{\rho}{\mu^2}\tan(\beta A_0^2 \rho t)(u_{KM}+1+\mu^2)(u_{KM}+1) = 0. \tag{38}$$

This can be integrated to give

$$u_{KM} = \mu^2 \frac{\cos(\beta A_0^2 \rho t)}{C_{KM}(y) - \cos(\beta A_0^2 \rho t)} - 1, \tag{39a}$$

$$v_{KM} = \rho \frac{\sin(\beta A_0^2 \rho t)}{C_{KM}(y) - \cos(\beta A_0^2 \rho t)}. \tag{39b}$$

$C_{KM}(y)$ is an integration constant and needs to satisfy

$$\frac{2\mu^2}{\rho^2} C_{KM}^2 - \frac{2\alpha}{\beta A_0^2 \rho^2}(\partial_y C_{KM})^2 = 1, \tag{40}$$

which gives

$$C_{KM} = \frac{\rho}{\sqrt{2}\mu}\cosh(K_\mu y), \tag{41}$$

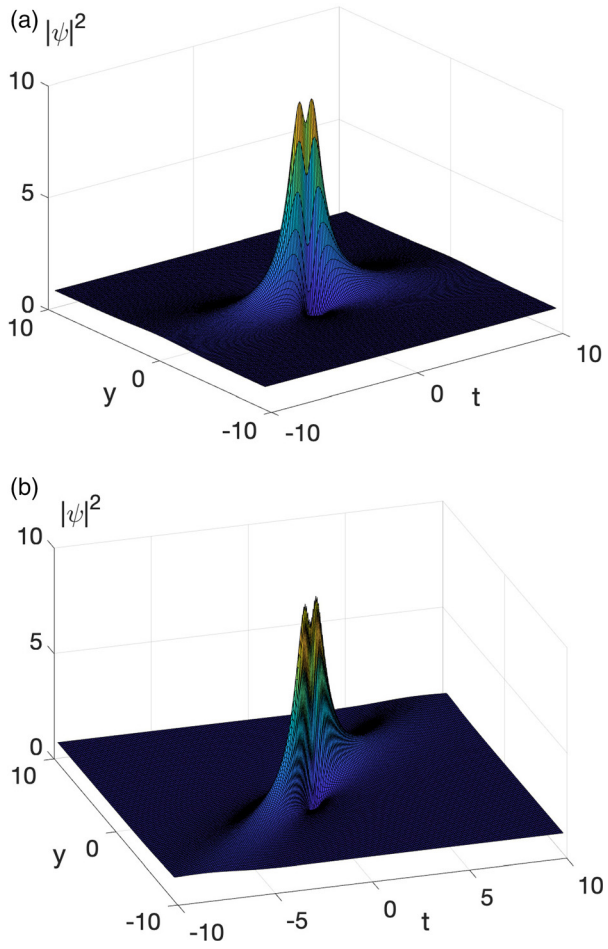

FIG. 7. The spatiotemporal landscape of the wave energy for Peregrine breathers. The excitation is localized both in time and space.

where $K_\mu = \mu\sqrt{\beta A_0^2/\alpha}$. Then, the nonlinear envelope is obtained as

$$\psi(y,t) = A_0 e^{i\beta A_0^2 t} \times \left(\frac{\sqrt{2}\mu^2\cos(\beta A_0^2\rho t) + i\sqrt{2}\rho\sin(\beta A_0^2\rho t)}{\sqrt{2+\mu^2}\cosh(K_\mu y) - \sqrt{2}\cos(\beta A_0^2\rho t)} - 1\right). \tag{42}$$

and the associated flux is given by

$$J_{KM} = 2\sqrt{2}\alpha A_0^2 \rho\sqrt{\mu^2+2}K_\mu \times \frac{\sinh(K_\mu y)\sin(\beta A_0^2\rho t)}{(\sqrt{2+\mu^2}\cosh(K_\mu y) - \sqrt{2}\cos(\beta A_0^2\rho t))^2}. \tag{43}$$

The typical spatiotemporal behavior is plotted in Fig. 8. The same normalization is used as before, and $\mu = 0.7$ is used. Here, we see the accumulation of energy in space at around $t = -5, 0, 5$. This is due to the accumulation of the flux, as shown in Fig. 8(b). Unlike Akhmediev breathers, this solution is localized in space, and the amplification repeats in time. As shown in the landscape (Fig. 9), this amplification

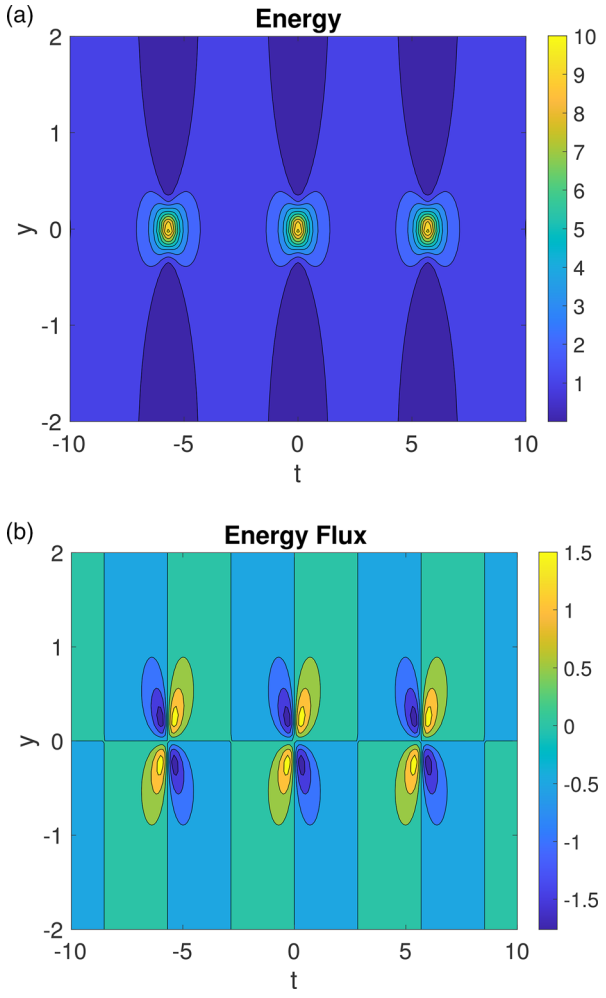

FIG. 8. The contour for the wave energy (a) and the energy flux (b) for Kuznetsov–Ma breathers. The flux accumulates in space, and this leads to the amplification of the energy. The events are localized in space and repeated in time.

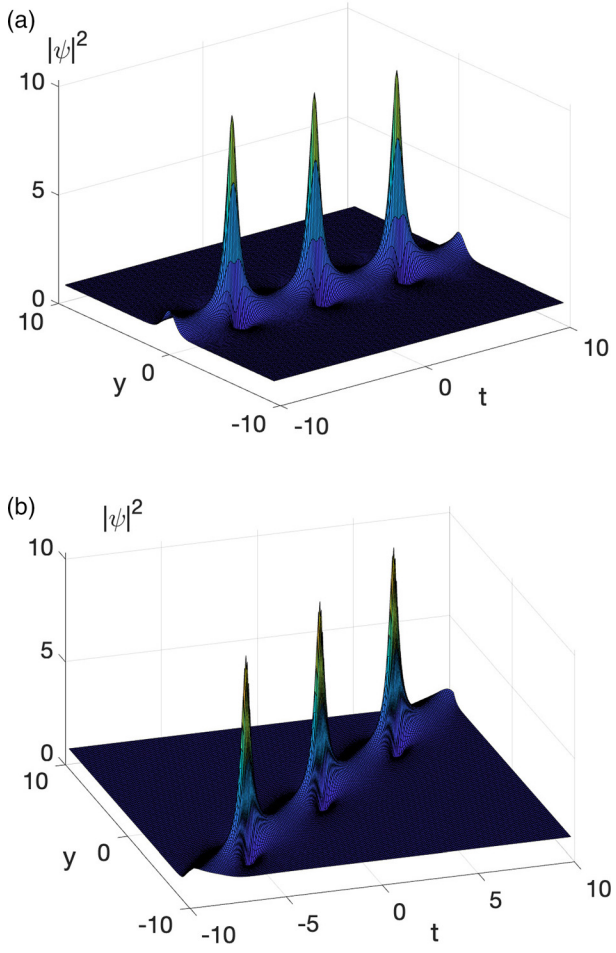

FIG. 9. The spatial–temporal landscape of the wave energy in the wave frame (a) and the laboratory frame (b). Kuznetsov–Ma breathers propagate at the group velocity. While propagating, the nonlinear wave "breathes" and changes its amplitude several times.

propagates at the group velocity. This nonlinear wave may be viewed as a special case of stably propagating soliton, although its amplitude oscillates in time.

As discussed here, several nonlinear waves can be excited in the framework of NLS (Table II). Given their different nature, these waves can be an origin of a rich variety of nonlinear evolution of plasmas. To elaborate this point, let us consider the nonlinear dynamics of excited patterns. Initially, the nonlinear interaction leads to the condensation of energy to pump large-scale structures. What would be a fate of this energy? One scenario is a realization of nonlinearly saturated, steady state. This may be achieved, for example, by the balance between the nonlinear driving force and stabilizing effect from wave dispersiveness. In this state, stably propagating soliton would be excited. More dynamical response is also possible. One case would be the oscillatory behavior, as exemplified by the Kuznetsov–Ma breathers. Accumulated energy is redistributed, and this process repeats in time. This is somewhat analogous to the predator–prey oscillation reported from drift wave-zonal flow system. Finally, a very unique nonlinear evolution is provided by the excitation of Akhmediev (and Peregrine) breathers. In this case, the excitation is localized in time and appears as a one-off event. The excitation of Akhmediev breather gives rise to a transient behavior of plasmas. In the rest of this work, we focus on this last example and provide an experimental evidence for its excitation.

D. Drift breathers in physical coordinates

In this work, we use the theoretical waveform [Eq. (28)] to identify breather excitation in experiments. To do so, here we describe how the wave appears for actual experimental parameters. We first note that the breather solution is obtained in the wave frame moving at the group velocity. The pattern in the laboratory frame is then recovered by setting $y \to y - v_{gr}t$, where $v_{gr} = \partial\omega/\partial k_y$ is the group velocity of drift wave. We also note that the coordinates used for reductive perturbation are those for slow evolution, and the original coordinates are

recovered by setting $y \to \epsilon y$ and $t \to \epsilon^2 t$, where ϵ is a small parameter. ϵ is typically on the order of normalized fluctuation amplitude. As an example, we consider a case of basic experiment, such as linear magnetized plasma experiment (PANTA). In these plasmas, $\rho_s \sim 1\,\mathrm{cm}$, $\omega_{*e}/(2\pi) \sim 1 - 10\,\mathrm{kHz}$, the poloidal mode number $m = 2 - 3$, $\tilde{n}/n_0 \sim 0.2 - 0.3$, etc. For representative values on PANTA, we have the coefficients for NLS as $\alpha = -10.1\,\mathrm{m}^2/\mathrm{s}$ and $\beta = -7.7 \times 10^5/\mathrm{s}$. Note that this is a modulationally unstable case, $\alpha\beta > 0$. The spatiotemporal energy landscape is given in Fig. 10(a). In this case, the accumulation of the wave energy appears at one location in space. The excitation event propagates in the positive azimuthal direction, which corresponds to the electron diamagnetic direction, at the group velocity. This behavior is quite distinctive as compared to the stably propagating envelope soliton, Fig. 10(b). Here, the envelope soliton solution is obtained by seeking for steadily propagating solution of the form of $A(y - c_1 t)$ and $\theta(y - c_2 t)$. Integrating NLS,[26] we have

$$\psi = A_0 \mathrm{dn}\left(A_0\sqrt{\frac{\beta}{2\alpha}}(y - c_1 t); k\right) \times \exp\left[i\left(\frac{c_1}{2\alpha}y + \left(\frac{\beta}{2}(a^2 + b^2) - \frac{c_1^2}{4\alpha}\right)t\right)\right]. \quad (44)$$

Here, dn is Jacobi elliptic function, a and b are the maximum and the minimum amplitude of the envelope, and $k^2 = 1 - b^2/a^2$. For $b \to 0$, $\mathrm{dn}(\ldots) \to 1/\cosh(\ldots)$, thus the well-known bright soliton solution[26] is recovered. Using the same parameters for Fig. 10(a), we have a typical spatiotemporal pattern of envelope soliton, as shown in Fig. 10(b). As compared to breather, the modulation amplitude is modest. The modulation also stably propagates. The propagation velocity c_1 can be determined from the periodic boundary condition in the space, which leads to $c_1 = v_{gr} + 2\alpha/L_n$. The propagation speed is different from that of breathers and can be even opposite to the group velocity, as is the case for the parameters chosen here. In this case, while the carrier drift wave propagates in the electron diamagnetic direction, the envelope soliton propagates in the ion diamagnetic direction. A similar behavior is reported in experiments.[14] Envelope solitons and breathers have very different features.

The temporal evolution of breather, including the contribution from the carrier oscillation, is shown in Fig. 11. Here, the modulation of the phase is also shown as a shift from the reference oscillation. The excitation of the breather leaves a footprint in the phase evolution, as indicated in red. The simultaneous modulation of amplitude and phase is visible for realistic experimental parameters, and we provide experimental evidence in Sec. III.

III. SEARCHING BREATHERS IN EXPERIMENT

In this section, we provide experimental evidence that drift waves can nonlinearly develop into breathers. Data are taken from the linear magnetized plasma experiment, PANTA.[55,56] Figure 12(a) provides a schematic view of the device. In PANTA, cylindrical plasmas are produced by the Helicon source at frequency of 7 MHz. The RF power can be varied as 1–6 kW. The magnetic field is in the z direction, and the strength is $B = 300$–1500 G. The discharge condition for the data

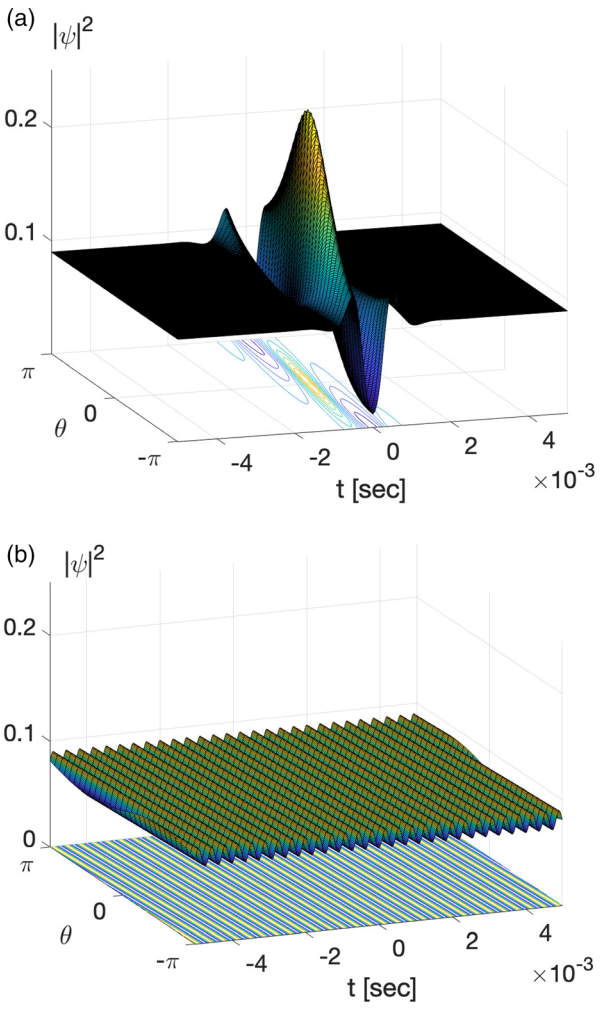

FIG. 10. The energy surface for typical parameters in basic experiments for breather (a) and for envelope soliton (b).

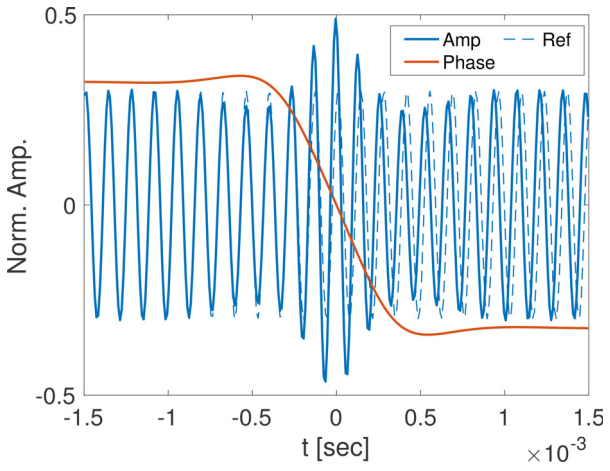

FIG. 11. The time evolution of the amplitude (blue) and the phase (red). The reference (dashed line) oscillation without modulation is also plotted.

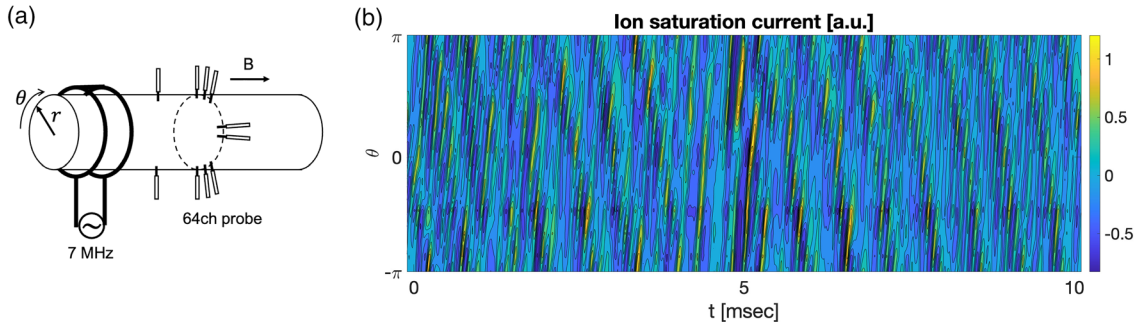

FIG. 12. Experimental setup and typical data in PANTA.

used in this work is as follows: RF power is 3 kW, $B = 900$ G, and the working gas is argon. In this condition, typical plasma parameters are as follows: the plasma radius ~5 cm, the plasma length ~4 m, the central density $n \sim 10^{18}\,\mathrm{m}^{-3}$, and the temperature $T_e \sim 3$ eV, respectively. In this condition, the density gradient builds up and drives drift waves unstable. Multiple probes are installed to obtain fluctuation data. In particular, a 64-channel probe array is installed at $z = 1.875$ m, with 64 probes azimuthally aligned at $r = 4$ cm. The 64 probes provide the ion saturation current I_{is} and the floating potential V_f sequentially. Figure 12(b) depicts a typical data obtained by the 64 channel probe. We seek for the breather excitation in these data. Note that this provides a unique environment to seek for the breather excitation in both spatial and temporal data. The flux associated with breather excitation can be also evaluated by using ion saturation current and floating potential. To complement the data obtained in the previous work, we use the probe shifted by 180° for a reference.

We start by searching drift breather in spatial data. Figure 13 describes a snapshot of spatial pattern. Here, the predicted waveform is given in blue, and the snapshot of experimental data is given in red. The 2 cases are shown for poor (Exp1) and good (Exp2) agreement, respectively. More quantitatively, we can calculate the correlation between the theory and experiment

$$C(t) = \frac{\int (d\theta/2\pi)\phi(\theta, t=0)\tilde{I}_{is}(\theta, t)}{\sqrt{\int (d\theta/2\pi)\phi^2(\theta, t=0)}\sqrt{\int (d\theta/2\pi)\tilde{I}_{is}^2(\theta, t)}}. \quad (45)$$

Here, ϕ is the theoretical waveform (including both envelope and carrier) and $\tilde{I}_{is}$ is the fluctuating component of ion saturation current ($\tilde{I}_{is} = I_{is} - \langle I_{is}\rangle_t - \langle I_{is}\rangle_\theta + \langle\langle I_{is}\rangle\rangle_{\theta,t}$ where $\langle\cdots\rangle_{t,\theta}$ is the time average and the azimuthal average, respectively, and $\langle\langle\cdots\rangle\rangle_{t,\theta}$ is the average over both time and azimuthal direction.). This correlation quantifies how the two spatial patterns resemble with each other. For the case shown in Fig. 13, $C(t) = 0.8051$ for the good agreement and $C(t) = 0.0052$ is for the poor case. In this work, we consider $C(t) > 0.7$ as a meaningful correlation.

A similar spatial pattern as breather can be detected by calculating the correlation. By repeating this for a given set of time series, we can analyze how often the similar pattern is excited in the experiment. Figure 14 describes the time series used for the analysis and how often the similar spatial pattern is excited. The normalized ion saturation current, $\tilde{I}_{is}/\langle\langle I_{is}\rangle\rangle_{\theta,t}$, is plotted for the time window of 60 ms, which corresponds to 6000 data points. The bottom graph shows the excitation index, which is calculated to be 1 for $C(t) > 0.7$ and 0 otherwise. The vertical line corresponds to the timing when the similar spatial pattern is detected. The excitation is randomly distributed, and thus,

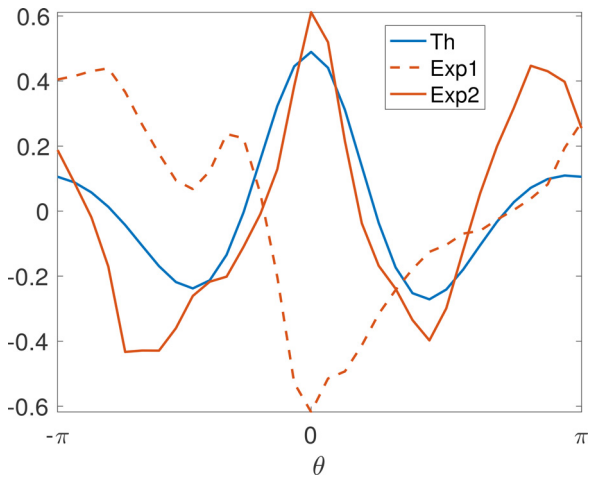

FIG. 13. Comparison of the spatial pattern. Correlation between the spatial patterns from theory and experiment is used to quantify the excitation.

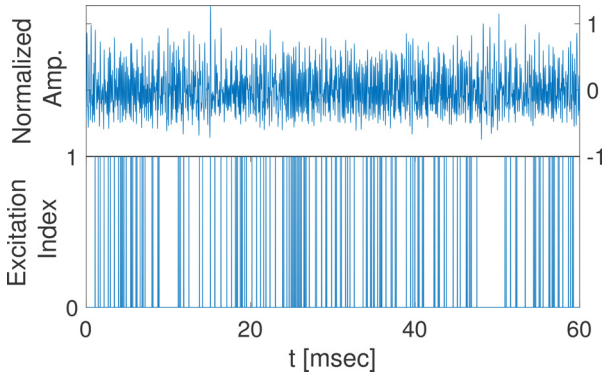

FIG. 14. Timings of the breather-like events detected via the spatial pattern matching.

the pattern is not due to the periodic propagation of a stable pattern. There is an interval with frequent excitation, which corresponds to the dense region, for example, around $t = 25$ ms, and a quiescent interval with scarce excitation (e.g., around $t = 10, 50$ ms). In total, we have detected 352 events.

The above analysis is based on the spatial pattern of the theoretical waveform and experimental data. More direct evidence of breather excitation can be found in the dynamical evolution of the wave pattern. To show the case of breather excitation in the time series, we average the time series by taking the timings of the spatial matching as a clock. Namely, when $C(t) > 0.7$, we take this time as an origin, t_0. By defining the time window $-\Delta t/2 < t - t_0 < \Delta t/2$, we correct the data within this window and average the corrected data over the excitation events. The result is shown in Fig. 15. Here, $\Delta t = 1.2$ ms. Figure 15(a) shows the spatial pattern averaged over the entire excitation events. The time evolution is given in Fig. 15(b). As discussed above, breather excitation leaves a footprint in the phase evolution as well. Evidence of this phase modulation is given in Fig. 15(c). While the compared data do not match exactly, theoretical prediction and experimental data do not contradict with each other. By providing the comparison from several aspects, our results are indicative of the excitation of drift breathers in actual experimental data.

We can evaluate more detailed features of drift breathers. While the normalized ion saturation current is used to demonstrate the excitation of drift breathers, we can also use floating potential to characterize breather dynamics. In PANTA, floating potential is measured by the probes adjacent to the probe for ion saturation current. By averaging floating potential data simultaneously, we can evaluate breather excitation with both the ion saturation current and floating potential, as shown in Fig. 16. Here, the normalized ion saturation current $\tilde{I}_{is}/\langle\langle I_{is}\rangle\rangle_{\theta,t}$ and the normalized floating potential $e\tilde{V}_f/T_e$ are plotted. The minus (plus) refers to the position in the negative (positive) azimuthal direction from the position for the I_{is} probe. First, we note that the ion saturation current and the floating potential exhibit a similar evolution. In terms of amplitude, the root mean square of the normalized ion saturation current is 0.14, while that for the normalized floating potential is 0.17. The amplitude is comparable, and hence, the density response is close to Boltzmann response. This is a typical feature of drift waves, and this feature also holds at the nonlinear stage that involves the excitation of breather. We also note that while the phase of the envelope of each quantity is modulated in a similar manner, there exists a finite relative phase shift between them. This gives rise to particle flux, as shown in Fig. 17. The radial particle flux is evaluated from $\Gamma_n = \langle\tilde{v}_r\tilde{n}\rangle \propto \langle\tilde{E}_\theta\tilde{n}\rangle$. The density fluctuation is obtained from the fluctuating ion saturation current, and the fluctuating azimuthal electric field is calculated from the difference between the floating potentials measured by the tips adjacent to the tip that is measuring the ion saturation current. The flux associated with the breather event (breather flux) is calculated by averaging the instantaneous flux over the excitation events. For comparison, we calculate the ordinary averaged flux (total flux) by averaging over the time and azimuthal direction. As shown in Fig. 17, we see that the flux is amplified during the breather excitation. The breather flux transiently exceeds the total flux, and the amplification factor can reach up to the factor of 6.

While this work presents evidence that drift breathers can be excited, this does not mean drift breathers are always excited. There are cases that drift wave does not develop into breathers and other nonlinear structures are excited. For example, we could not find a meaningful correlation for the data used in the reference.[14] The condition for the excitation may be related to the existence condition of the

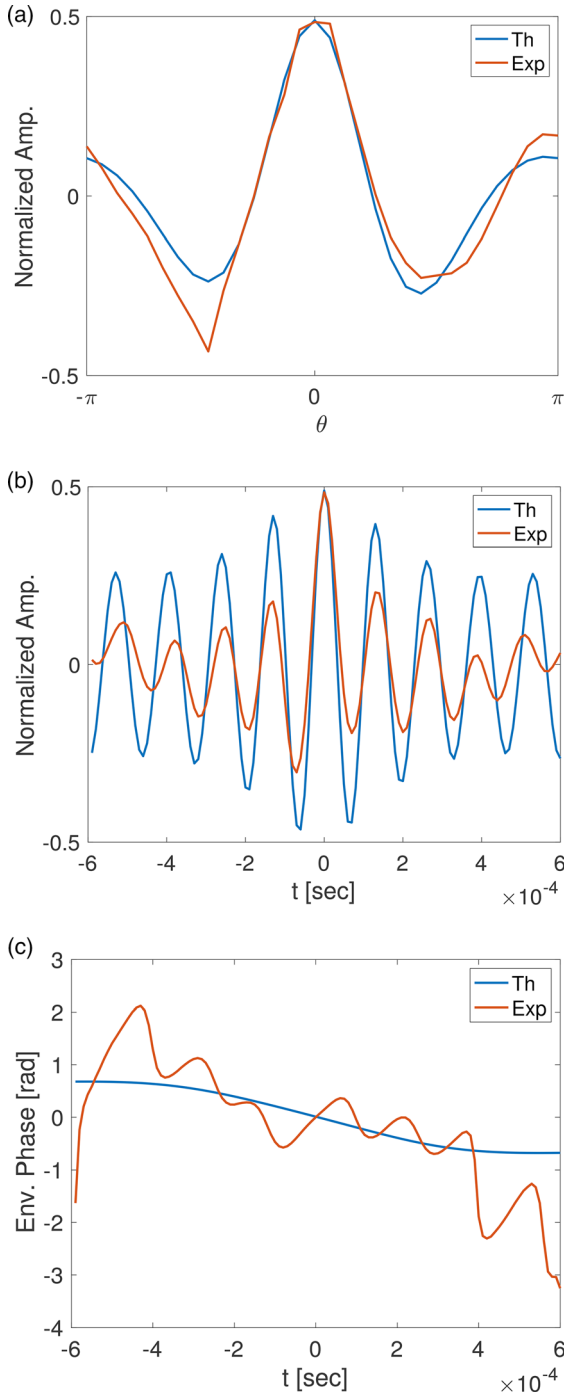

FIG. 15. Comparison between theory and experiment for amplitude and phase. Here, the evolution is averaged over the excitation events.

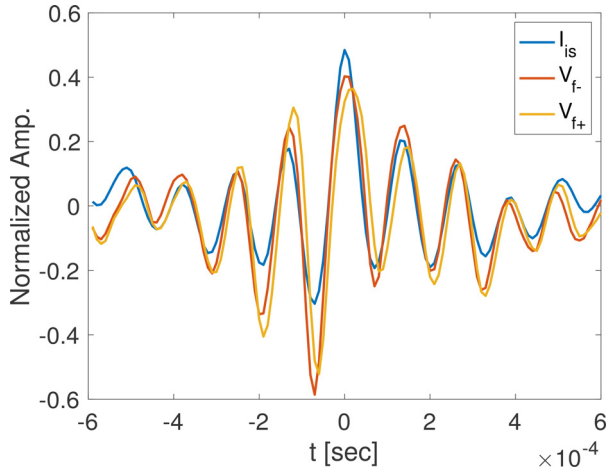

FIG. 16. Ion saturation current and floating potential. The response is close to Boltzmann.

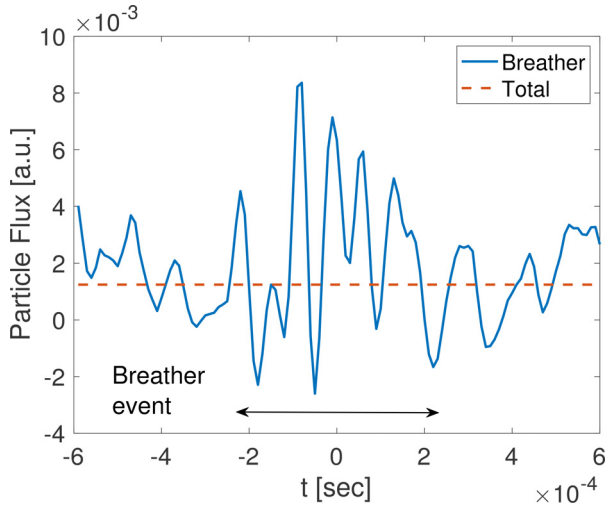

FIG. 17. Flux associated with breather event.

nonlinear waveform, $\nu^2 < 2$. Rewriting this in terms of physical parameters, the condition is given by

$$A_0 > \sqrt{\frac{\alpha}{\beta}}\frac{K}{\sqrt{2}}. \tag{46}$$

Thus, the background oscillation of drift wave needs to be strong enough to exceed the critical value, which is determined by the competition between the nonlinearity and the dispersiveness of drift waves. Using typical values for the data used in this paper, we find that $A_{crit} = 0.29$. Since the typical amplitude of the fluctuation data is on the order of $A_0 \sim 0.2$–0.3, the condition can be satisfied and the excitation of drift breathers is likely. On the other hand, if we use the value from,[14] we find $A_{crit} = 0.93$. This is too large to be overcome, and indeed, we could not find a meaningful correlation in such a case. These are consistent with the above condition, and thus, the drift breather excitation is likely when the background drift wave amplitude is large enough.

IV. CONCLUSION AND DISCUSSION

In conclusion, this paper presents evidence for drift waves that can nonlinearly develop into breathers, as reported from ocean and optics. Its excitation is formulated by modulational analysis, which describes the excitation of breathers via nonlinear Schrödinger equation (NLS) for envelope. The exact nonlinear solutions for NLS are obtained and describe the various transient excitations of nonlinear breathers. While the wave envelope grows via modulational instability, this growth terminates and the accumulated wave energy is spatially redistributed. This is a general consequence of the nonlinear time evolution for 1D NLS without collapse and the sign of the wave energy flux flips at the later stage of the nonlinear evolution. The entire dynamics can be viewed as a transient increase in the wave amplitude. The amplification ranges from 1 to 3. While the breather excitation is often sought for in the amplitude modulation, the phase of the envelope is modulated. The simultaneous modulation of the amplitude and phase is used as evidence for the breather excitation in experimental data. In this work, the excitation of drift breathers is confirmed in the data obtained from the linear magnetized plasma experiment, PANTA. The spatial pattern was used as an indicator for the excitation of a similar pattern, and the excitation is quantified by calculating the correlation between the theoretical spatial pattern and the experimentally observed pattern by the multi-point probe measurement. A similar pattern randomly appears, and we have detected 352 events in 6000 data points (60 ms). By averaging over this, we have extracted the typical time evolution for the wave amplitude and the phase. The results indicate the excitation of drift breathers. Once excited, drift breather transiently increases the transport flux. The excitation of drift breather is likely when the existence condition for the nonlinear waveform is satisfied.

While this work discusses the excitation of drift breathers, there are aspects that the present study does not address. In this work, we have demonstrated the excitation of drift breathers by using Eq. (28). NLS, however, admits other nonlinear solutions such as Eq. (42). Super-rogue waves with even higher amplitude are also reported.[62] The excitation of other types of nonlinear drift breathers [e.g., Eq. (42)] may be possible, and this will be analyzed by using the different spatiotemporal pattern for calculating the correlation between the theoretical waveform and experimental data. Here, the selection rule, that is, why one solution is selected over the others, will be also studied. We also note that application to fusion problems awaits further studies. Although we have briefly discussed the impact of breather excitation on transport flux, more studies are of course required. For example, the transient feature of the breather excitation is amenable to the intermittent feature of fusion turbulence.[63,64] This point will be elaborated further in the future. Breather excitation may be also related to the sudden release of stored free energy.[22,40,65] Detailed studies that address the relevance of breathers as compared to other mechanisms based on MHD instabilities will be discussed elsewhere. Finally, the feedback of the excitation of drift breather on the background plasmas is also an important issue. In experiments, while the excitation of breathers relaxes the background density profile, the profile builds up due to the finite plasma source. The profile dynamics feeds back to the original model through coefficients. The simultaneous evolution of the

wave amplitude and the background density profile may be formulated in a similar manner that is developed for the front propagation.[66]

ACKNOWLEDGMENTS

We thank H. Tsuji, K. Terasaka, and H. Arakawa for useful discussion. This work is partly supported by the Grants-in-Aid for Scientific Research of JSPS of Japan (Nos. JP18K03578, JP21H01066, and JP17H06089), the joint research project in RIAM, Kyushu University.

AUTHOR DECLARATIONS

Conflict of Interest

The authors have no conflicts to disclose.

Author Contributions

Yusuke Kosuga: Conceptualization (lead); Formal analysis (lead); Writing – original draft (lead). **Shigeru Inagaki:** Data curation (equal); Investigation (equal); Validation (equal); Writing – review & editing (equal). **Yuichi Kawachi:** Data curation (equal); Investigation (equal); Writing – review & editing (equal).

DATA AVAILABILITY

The data that support the findings of this study are available from the corresponding author upon reasonable request.

REFERENCES

[1]H. K. Moffatt, *Magnetic Field Generation in Electrically Conducting Fluids* (Cambridge University Press, Cambridge, 1978).
[2]P. Tzeferacos, A. Rigby, A. F. A. Bott, A. R. Bell, R. Bingham, A. Casner, F. Cattaneo, E. M. Churazov, J. Emig, F. Fiuza *et al.*, Nat. Commun. **9**, 591 (2018).
[3]C. Joshi and V. Malka, New J. Phys. **12**, 045003 (2010).
[4]A. Hasegawa, C. G. Maclennan, and Y. Kodama, Phys. Fluids **22**, 2122 (1979).
[5]M. N. Rosenbluth and F. L. Hinton, Phys. Rev. Lett. **80**, 724 (1998).
[6]P. H. Diamond, M. N. Rosenbluth, E. Sanchez, C. Hidalgo, B. V. Milligen, T. Estrada, B. Branas, M. Hirsch, H. J. Hartfuss, and B. A. Carreras, Phys. Rev. Lett. **84**, 4842 (2000).
[7]P. H. Diamond, S.-I. Itoh, K. Itoh, and T. S. Hahm, Plasma Phys. Controlled Fusion **47**, R35 (2005).
[8]A. Fujisawa, K. Itoh, H. Iguchi, K. Matsuoka, S. Okamura, A. Shimizu, T. Minami, Y. Yoshimura, K. Nagaoka, C. Takahashi *et al.*, Phys. Rev. Lett. **93**, 165002 (2004).
[9]P. H. Diamond, A. Hasegawa, and K. Mima, Plasma Phys. Controlled Fusion **53**, 124001 (2011).
[10]L. Schmitz, L. Zeng, T. L. Rhodes, J. C. Hillesheim, E. J. Doyle, R. J. Groebner, W. A. Peebles, K. H. Burrell, and G. Wang, Phys. Rev. Lett. **108**, 155002 (2012).
[11]G. S. Xu, B. N. Wan, H. Q. Wang, H. Y. Guo, H. L. Zhao, A. D. Liu, V. Naulin, P. H. Diamond, G. R. Tynan, M. Xu *et al.*, Phys. Rev. Lett. **107**, 125001 (2011).
[12]I. Cziegler, A. E. Hubbard, J. W. Hughes, J. L. Terry, and G. R. Tynan, Phys. Rev. Lett. **118**, 105003 (2017).
[13]Y. Kosuga, F. Kin, and M. Sasaki, Contrib. Plasma Phys. **60**, e201900141 (2020).
[14]T. Yamada, S. I. Itoh, T. Maruta, N. Kasuya, Y. Nagashima, S. Shinohara, K. Terasaka, M. Yagi, S. Inagaki, Y. Kawai *et al.*, Nat. Phys. **4**, 721 (2008).
[15]T. Yamada, S. I. Itoh, S. Inagaki, Y. Nagashima, N. Kasuya, K. Kamataki, H. Arakawa, T. Kobayashi, M. Yagi, A. Fujisawa *et al.*, Phys. Rev. Lett. **105**, 225002 (2010).
[16]S. Inagaki, T. Tokuzawa, K. Itoh, K. Ida, S. I. Itoh, N. Tamura, S. Sakakibara, N. Kasuya, A. Fujisawa, S. Kubo *et al.*, Phys. Rev. Lett. **107**, 115001 (2011).
[17]F. Kin, A. Fujisawa, K. Itoh, Y. Kosuga, M. Sasaki, S. Inagaki, Y. Nagashima, T. Yamada, N. Kasuya, K. Yamasaki *et al.*, Phys. Plasmas **26**, 042306 (2019).
[18]S. Champeaux and P. H. Diamond, Phys. Lett. A **288**, 214 (2001).
[19]J. A. Krommes and C.-B. Kim, Phys. Rev. E **62**, 8508 (2000).
[20]G. Manfredi, C. M. Roach, and R. O. Dendy, Plasma Phys. Controlled Fusion **43**, 825 (2001).
[21]Y. Kosuga and K. Hasamada, Phys. Plasmas **25**, 100701 (2018).
[22]J. E. Lee, G. S. Yun, W. Lee, M. H. Kim, M. Choi, J. Lee, M. Kim, H. K. Park, J. G. Bak, W. H. Ko *et al.*, Sci. Rep. **7**, 45075 (2017).
[23]J. Cheng, J. Q. Dong, K. Itoh, S.-I. Itoh, L. W. Yan, J. Q. Xu, M. Jiang, Z. H. Huang, K. J. Zhao, Z. B. Shi *et al.*, Nucl. Fusion **60**, 046021 (2020).
[24]G. Dif-Pradalier, G. Hornung, P. Ghendrih, Y. Sarazin, F. Clairet, L. Vermare, P. H. Diamond, J. Abiteboul, T. Cartier-Michaud, C. Ehrlacher *et al.*, Phys. Rev. Lett. **114**, 085004 (2015).
[25]A. Ashourvan, R. Nazikian, E. Belli, J. Candy, D. Eldon, B. A. Grierson, W. Guttenfelder, S. R. Haskey, C. Lasnier, G. R. McKee *et al.*, Phys. Rev. Lett. **123**, 115001 (2019).
[26]A. Scott, *Nonlinear Science* (Oxford University Press, 2003).
[27]H. Ikezi, R. J. Taylor, and D. R. Baker, Phys. Rev. Lett. **25**, 11 (1970).
[28]K. Nozaki, T. Taniuti, and K. Watanabe, J. Phys. Soc. Jpn **46**, 991 (1979).
[29]F. Kin, K. Itoh, A. Fujisawa, Y. Kosuga, M. Sasaki, T. Yamada, S. Inagaki, S. I. Itoh, T. Kobayashi, Y. Nagashima *et al.*, Phys. Plasmas **25**, 062304 (2018).
[30]M. Onorato, S. Residori, U. Bortolozzo, A. Montina, and F. T. Arecchi, Phys. Rep. **528**, 47 (2013).
[31]V. E. Zakharov and L. A. Ostrovsky, Physica D **238**, 540 (2009).
[32]A. Chabchoub, N. P. Hoffmann, and N. Akhmediev, Phys. Rev. Lett. **106**, 204502 (2011).
[33]M. Shats, H. Punzmann, and H. Xia, Phys. Rev. Lett. **104**, 104503 (2010).
[34]D. R. Solli, C. Ropers, P. Koonath, and B. Jalali, Nature **450**, 1054 (2007).
[35]H. Bailung, S. K. Sharma, and Y. Nakamura, Phys. Rev. Lett. **107**, 255005 (2011).
[36]W. M. Moslem, R. Sabry, S. K. El-Labany, and P. K. Shukla, Phys. Rev. E **84**, 066402 (2011).
[37]M. McKerr, I. Kourakis, and F. Haas, Plasma Phys. Controlled Fusion **56**, 035007 (2014).
[38]M. McKerr, F. Haas, and I. Kourakis, Phys. Plasmas **23**, 052120 (2016).
[39]G. P. Veldes, J. Borhanian, M. McKerr, V. Saxena, D. J. Frantzeskakis, and I. Kourakis, J. Opt. **15**, 064003 (2013).
[40]K. Ida, T. Kobayashi, K. Itoh, M. Yoshinuma, T. Tokuzawa, T. Akiyama, C. Moon, H. Tsuchiya, S. Inagaki, and S.-I. Itoh, Sci. Rep. **6**, 36217 (2016).
[41]R. J. Goldston, Nucl. Fusion **52**, 013009 (2012).
[42]P. A. Politzer, Phys. Rev. Lett. **84**, 1192 (2000).
[43]B. V. Compernolle and G. J. Morales, Phys. Plasmas **24**, 112302 (2017).
[44]M. J. Choi, H. Jhang, J.-M. Kwon, J. Chung, M. Woo, L. Qi, S. Ko, T.-S. Hahm, H. K. Park, H.-S. Kim *et al.*, Nucl. Fusion **59**, 086027 (2019).
[45]J. A. Boedo, D. L. Rudakov, R. A. Moyer, G. R. McKee, R. J. Colchin, M. J. Schaffer, P. G. Stangeby, W. P. West, S. L. Allen, T. E. Evans *et al.*, Phys. Plasmas **10**, 1670 (2003).
[46]G. Y. Antar, J. H. Yu, and G. Tynan, Phys. Plasmas **14**, 022301 (2007).
[47]T. A. Carter, Phys. Plasmas **13**, 010701 (2006).
[48]Ö. D. Gürcan and P. H. Diamond, J. Phys. A **48**, 293001 (2015).
[49]Y. Kosuga, Phys. Plasmas **24**, 122305 (2017).
[50]Y. Zhou, H. Zhu, and I. Y. Dodin, Plasma Phys. Controlled Fusion **61**, 075003 (2019).
[51]H. Zhu and I. Y. Dudin, Phys. Plasmas **28**, 032303 (2021).
[52]B. Kibler, J. Fatome, C. Finot, G. Millot, F. Dias, G. Genty, N. Akhmediev, and J. M. Dudley, Nat. Phys. **6**, 790 (2010).
[53]G. Clauss, M. Klein, and M. Onorato, in *Proceedings of the ASME 2011 30th International Conference on Ocean, Offshore and Arctic Engineering* (Rotterdam, The Netherlands, 2011), pp. 1–13.
[54]B. Kibler, J. Fatome, C. Finot, G. Millot, G. Genty, B. Wetzel, N. Akhmediev, F. Dias, and J. M. Dudley, Sci. Rep. **2**, 463 (2012).
[55]S. Inagaki, T. Kobayashi, Y. Kosuga, S.-I. Itoh, T. Mitsuzono, Y. Nagashima, H. Arakawa, T. Yamada, Y. Miwa, N. Kasuya *et al.*, Sci. Rep. **6**, 22189 (2016).
[56]Y. Kawachi, S. Inagaki, F. Kin, K. Yamasaki, Y. Kosuga, M. Sasaki, Y. Nagashima, T. Yamada, H. Arakawa, N. Kasuya *et al.*, Plasma Phys. Controlled Fusion **62**, 055011 (2020).
[57]R. C. Davidson, *Methods in Nonlinear Plasma Theory* (Academic Press, New York, 1972).

[58]E. Kartashova and I. V. Shugan, Europhys. Lett. **95**, 30003 (2011).
[59]B. A. Trubnikov and S. K. Zhdanov, Phys. Rep. **155**, 137 (1987).
[60]S. I. Krasheninnikov, A. I. Smolyakov, Y. Zhang, and O. Chapurin, Phys. Plasmas **28**, 010702 (2021).
[61]P. A. Robinson, Rev. Mod. Phys. **69**, 507 (1997).
[62]A. Chabchoub, N. Hoffmann, M. Onorato, and N. Akhmediev, Phys. Rev. X **2**, 011015 (2012).
[63]U. Frisch, *Turbulence: The Legacy of A. N. Kolmogorov* (Cambridge University Press, Cambridge, 2010).
[64]B. A. Carreras, L. Garcia, J. H. Nicolau, B. P. van Milligen, U. Hoefel, M. Hirsch, and TJ-II and W7-X Teams, Plasma Phys. Controlled Fusion **62**, 025011 (2020).
[65]H. Zohm, Plasma Phys. Controlled Fusion **38**, 105 (1996).
[66]X. Garbet, Y. Sarazin, F. Imbeaux, P. Ghendrih, C. Bourdelle, O. D. Gurcan, and P. H. Diamond, Phys. Plasmas **14**, 122305 (2007).